Low Temperature Physics/Fizika Nizkikh Temperatur, 2013, v. 39, No. 9, pp. 1021–1030

Excitation spectrum in two-dimensional superfluid ^{4}He

F. Arrigoni, E. Vitali, D.E. Galli, and L. Reatto

Dipartimento di Fisica, Università degli Studi di Milano, 16 Celoria Via, Milano 20133, Italy
E-mail: Davide.Galli@unimi.it; davidemilio.galli@gmail.com

Received March 14, 2013

In this work we perform an *ab-initio* study of an ideal two-dimensional sample of ^{4}He atoms, a model for ^{4}He films adsorbed on several kinds of substrates. Starting from a realistic hamiltonian we face the microscopic study of the excitation phonon–roton spectrum of the system at zero temperature. Our approach relies on path integral ground state Monte Carlo projection methods, allowing to evaluate exactly the dynamical density correlation functions in imaginary time, and this gives access to the dynamical structure factor of the system $S(q,\omega)$, containing information about the excitation spectrum $E(q)$, resulting in sharp peaks in $S(q,\omega)$. The actual evaluation of $S(q,\omega)$ requires the inversion of the Laplace transform in ill-posed conditions, which we face via the genetic inversion via falsification of theories technique. We explore the full density range from the region of spinodal decomposition to the freezing density, i.e., 0.0321 Å^{-2}– 0.0658 Å^{-2}. In particular we follow the density dependence of the excitation spectrum, focusing on the low-wave vector behavior of $E(q)$, the roton dispersion, the strength of single quasiparticle peak, $Z(q)$, and the static density response function, $\chi(q)$. As the density increases, the dispersion $E(q)$ at low-wave vector changes from a superlinear (anomalous dispersion) trend to a sublinear (normal dispersion) one, anticipating the crystallization of the system; at the same time the maxon–roton structure, which is barely visible at low density, becomes well developed at high densities and the roton wave vector has a strong density dependence. Connection is made with recent inelastic neutron scattering results from highly ordered silica nanopores partially filled with ^{4}He.

PACS: 67.25.bh Films and restricted geometries;
67.25.dt Sound and excitations.

Keywords: superfluidity, two-dimensional quantum fluids, elementary excitations, roton.

1. Introduction

Helium exists in two stable isotopes, ^{4}He and ^{3}He, which differ for their nuclear spin: ^{4}He atoms are bosons with nuclear spin $I = 0$, while ^{3}He atoms are fermions with nuclear spin $I = 1/2$. The effective interaction among helium atoms is well described by a hard core potential plus an attraction arising from zero-point fluctuations in the charge distribution. The interaction results in a simple Lennard–Jones-like two-body spherically symmetric potential $v(r)$, for which accurate analytical expressions are known [1]. The hamiltonian of the bulk system reads:

$$\hat{H} = -\frac{\hbar^2}{2m}\sum_{i=1}^{N}\nabla_i^2 + \sum_{i<j=1}^{N} v(|\hat{\mathbf{r}}_i - \hat{\mathbf{r}}_j|) \qquad (1)$$

where m is the mass of ^{4}He atoms. Despite its very simple structure, helium exhibits numerous exotic phenomena in condensed form, whose theoretical explanation, in some aspects, is still a big challenge nowadays. Along with the many fascinating physical features related to the well-known phenomenon of superfluidity [2], which have been the object of several theoretical and experimental efforts, a unique fingerprint of such a system is the *spectrum* $E(q)$ of the elementary excitations.

Excitations in ^{4}He bulk systems have been extensively investigated after Landau's original conjecture [3] about the phonon–roton dispersion relation $E(q)$ and its connection with the definition of superfluidity in terms of a critical velocity. In 1953 Feynman showed that the shape of the phonon–roton spectrum can be justified on a quantum mechanical basis, relying on Bose statistics together with hard-core interactions [4]. Moreover, he suggested that the excitation spectrum of superfluid ^{4}He may be investigated by inelastic neutron scattering experiments. This was realized only almost one decade later [5], beautifully confirming the original Landau's guess. Actually, within the first Born approximation, the differential cross section in a thermal neutron scattering experiment on a sample of ^{4}He atoms, apart from kinematical factors, is provided by the *dynamical structure factor*:

$$S(q,\omega) = \frac{1}{2\pi N}\int_{-\infty}^{+\infty} dt\, e^{i\omega t}\langle e^{i\frac{t}{\hbar}\hat{H}}\hat{\rho}_{\mathbf{q}}e^{-i\frac{t}{\hbar}\hat{H}}\hat{\rho}_{-\mathbf{q}}\rangle \qquad (2)$$

where the brakets indicate a ground state or a thermal average, $\hat{H}$ is the Hamiltonian of the helium system (1), and $\hat{\rho}_{\mathbf{q}} = \sum_{i=1}^{N} \exp(-i\mathbf{q}\cdot\hat{\mathbf{r}}_i)$, $\hat{\mathbf{r}}_i$ being the position operator of the ith ^{4}He atom, is the local density operator in Fourier space. Sharp peaks in ω of $S(q,\omega)$ provide the spectrum of the elementary excitations of the system.

On the theoretical side, a systematic effort has been devoted to pursue an accurate description of the elementary excitations of the system. The original idea of Feynman–Cohen [6] of introducing back–flow correlations to improve variational excited states wave functions (later on extended by the correlated–basis–functions strategy [7]), has flown into the excited states shadow wave functions (SWF) technique [8]; SWF reproduced the experimental bulk dispersion relation $E(q)$ up to a high accuracy level [9] and even confirmed [9,10] the physical picture of a roton as a microscopic smoke ring [11]. A further turn in the study of excited states of superfluid ^{4}He was given by the advent of exact simulation methods for interacting Bose particles. It is not yet possible to perform a direct exact computation of excited states due to the sign problem. However, it is possible to extract dynamical properties from exact correlation functions in imaginary time [12]. This has been worked out by path integral Monte Carlo (PIMC) at finite temperature [13] or by ground state Monte Carlo [14,15] at T = 0 K. Indeed, such functions contain information on excited states of the system. In particular the density correlation function is related to $S(q,\omega)$ by an inverse Laplace transform. Due to discretization and statistical noise, the mathematical problem of extracting $S(q,\omega)$ is ill-posed, but powerful inversion methods have been introduced recently [15,16] and reliable results on the excitation spectrum of superfluid ^{4}He have been obtained [15,17,18].

Bosons in two dimensions (2D) are of great theoretical interest because the standard scenario of superfluidity associated with Bose-Einstein condensation (BEC) is not appropriate. In fact, in 2D and in almost 2D systems the order parameter, i.e., the condensate wave function, $\psi(\mathbf{r})$, vanishes at any finite temperature for a bulk system. The notion of long range order is replaced by that of topological long range order [19] with correlation function of the local order parameter decaying algebraically very slowly to zero. Notwithstanding a vanishing order parameter, a superfluid response is theoretically predicted up to a temperature where vortex and antivortex pairs unbind. These predictions have been beautifully confirmed by experiments [20]. Therefore a 2D Helium system is an interesting microscopic model for quasi-two-dimensional many-body quantum systems [21,22]: helium films on suitable substrates. For most substrates the interaction potential between the helium atoms and the substrate is much stronger (as it is the case of He–graphite interaction) than the He–He interaction and the helium atoms are adsorbed in a well-defined layer structure. Typically, only the first or the first two layers are strongly influenced by the details of the helium–substrate interaction. Several different physical realizations of substrates have been investigated, both in experimental and in theoretical works. For many substrates the closest He atoms to the substrate are disordered and localized, they form what the experimentalists call a "dead layer". Beyond that the first layer of mobile atoms are superfluid and can be well represented by a strictly 2D model. The experimental study of $S(q,\omega)$ of this film has shown the existence of elementary excitations with a phonon–maxon–roton structure [23]. A favorite substrate for adsorption studies is graphite because it offers rather extended regions of perfectly flat basal planes. At first sight this might be considered as an ideal situation for using the 2D model. This is not so for the first adsorbed layer because the adsorption potential is strongly corrugated. The consequence of the corrugation is that at low temperature the ^{4}He atoms form an ordered structure, either a triangular lattice that is commensurate with the substrate or, at higher coverage, an incommensurate triangular solid [24]. Experimentally no evidence has been found for superfluidity in the first adsorbed layer on graphite. Superfluidity has been found only in additional layers for which the 2D model can be used as a reasonable approximation.

Computation of the spectrum of elementary excitations of ^{4}He is of interest on one hand to uncover the dependence of rotons on the dimensionality of the system. On the other hand, this theoretical input is useful for the interpretation of scattering experiments from adsorbed ^{4}He.

Excitations for 2D ^{4}He have been studied by correlated basis function theory [25]. As far as we know, the only existing *ab initio* quantum Monte Carlo (QMC) calculation of excitations in 2D ^{4}He has been performed with variational theory using shadow wave functions [26]. As mentioned above exact QMC techniques are able to give access to estimations of $S(q,\omega)$ via exact calculations of dynamical correlation functions in imaginary time. The path integral ground state (PIGS) method [27] and in particular the shadow path integral ground state (SPIGS) method [28,29] together with the genetic inversion via falsification of theories (GIFT) method [15] have been applied to bulk ^{4}He systems [15,17], to adsorbed ^{4}He systems [18] and even to a pure 2D ^{3}He system [30] (via a quite sophisticated novel strategy). Here we apply such approaches to address the calculation of dynamical properties of a pure 2D ^{4}He system at zero temperature.

The article is structured as follows: in the next section we sketch the methodology; in Sec. 3 we present and discuss the results and our conclusions are in Sec. 4. In the Appendix we give the results of a variational computation of the ground state properties of ^{4}He in 2D based on SWF that are a byproduct of the exact SPIGS computation of Sec. 3.

2. Methodology

We focus thus on a strictly 2D collection of N structureless spinless bosons at zero temperature. The hamiltonian operator is (1). We let $\psi_0(\mathcal{R})$ be the ground state of $\hat{H}$, where we use the notation $\mathcal{R} = (\mathbf{r}_1,\ldots,\mathbf{r}_N)$.. The basic relation underlying QMC projection methods is the following:

$$\psi_0(\mathcal{R}) \propto \lim_{\lambda\to+\infty} \exp(-\lambda\hat{H})\psi_T(\mathcal{R}) \tag{3}$$

where $\psi_T(\mathcal{R})$ is any many-body wave function with non-zero overlap on $\psi_0(\mathcal{R})$. The operator $\exp(-\lambda\hat{H})$ can be seen as the evolution operator, $\exp(-i(t/\hbar)\hat{H})$, written for imaginary times; in this way, $\psi_0(\mathcal{R})$ turns out to be the limit of the imaginary time evolution of $\psi_T(\mathcal{R})$, with λ playing the role of imaginary time. A Trotter decomposition:

$$\mathrm{e}^{-\lambda\hat{H}} = (\mathrm{e}^{-\delta\tau\hat{H}})^M, \quad \delta\tau = \frac{\lambda}{M} \tag{4}$$

together with an (analytical or numerical) approximation for the imaginary time propagator:

$$\langle\mathcal{R}\,|\,\mathrm{e}^{-\delta\tau\hat{H}}\,|\,\mathcal{R}'\rangle = \mathcal{G}(\mathcal{R},\mathcal{R}',\delta\tau) + \mathcal{O}(\delta\tau^m) \tag{5}$$

where the order m depends on the approximation, allows to build up an approximate expression for the ground state wave function of the form:

$$\psi_0(\mathcal{R}) \simeq \int d\{\mathcal{R}_i\}\mathcal{G}(\mathcal{R},\mathcal{R}_1,\delta\tau)\ldots\mathcal{G}(\mathcal{R}_{M-1},\mathcal{R}_M,\delta\tau)\psi_T(\mathcal{R}_M) \tag{6}$$

where we have omitted an overall normalization factor. Any expectation value of an operator diagonal in coordinate representation (or of the Hamiltonian operator):

$$\langle\psi_0\,|\hat{O}\,|\,\psi_0\rangle \tag{7}$$

is expressed as a multidimensional average of a function $O(\mathcal{R})$ over a probability density of the form:

$$p(\{\mathcal{R}_i\}) = \frac{1}{\mathcal{Z}}\psi_T(\mathcal{R}_1)\prod_{i=1}^{2M}\mathcal{G}(\mathcal{R}_i,\mathcal{R}_{i+1},\delta\tau)\psi_T(\mathcal{R}_{2M}) \tag{8}$$

which can be sampled using Metropolis algorithm. The results can be considered exact in the sense that the errors arising from approximations can be reduced under the level of the statistical noise via a suitable choice of the time step $\delta\tau$ and the total projection time $\lambda = M\delta\tau$. Of course this also assumes that the results, for large enough λ, are independent on the choice of ψ_T. This has been verified [31], even by starting with ψ_T of a liquid for the solid phase or of a solid for a liquid phase one finds convergence to the correct result. Notwithstanding this, a judicious choice of ψ_T is important to accelerate convergence of ψ_T to ψ_0, i.e., a smaller value of λ is needed, and to reduce the variance of the results. What has been described here is the PIGS method, or the SPIGS method if ψ_T is a SWF.

This calculation scheme can be straightforwardly generalized to evaluate dynamical imaginary time correlation functions:

$$\langle\psi_0\,|\,\mathrm{e}^{\tau\hat{H}}\hat{O}\,\mathrm{e}^{-\tau\hat{H}}\hat{O}^\dagger\,|\,\psi_0\rangle. \tag{9}$$

The particular choice:

$$F(\mathbf{q},\tau) = \langle\psi_0\,|\,\mathrm{e}^{\tau\hat{H}}\,\hat{\rho}_{\mathbf{q}}\,\mathrm{e}^{-\tau\hat{H}}\,\hat{\rho}_{-\mathbf{q}}\,|\,\psi_0\rangle \tag{10}$$

provide the intermediate scattering function in imaginary time, which is related to the dynamical structure factor by the relation:

$$F(q,\tau) = \int_0^{+\infty} d\omega\,\mathrm{e}^{-\tau\omega}S(q,\omega). \tag{11}$$

Thus, the estimation of $S(q,\omega)$ requires to invert the integral relation (11) in ill-posed conditions, since $F(q,\tau)$ is known only on a discrete and finite set of instants τ (typically $\tau = n\delta\tau$, $n = 0,\ldots,\bar{n}$) and is affected by a statistical uncertainty arising from the stochastic Monte Carlo calculation. Despite the well-known difficulties related to the inversion of the Laplace transform in ill-posed conditions, the evaluation of $S(q,\omega)$ starting from the QMC estimation of $F(\mathbf{q},\tau)$ (10) has been proved to be fruitful for several bosonic systems using a recent technique GIFT [15]. GIFT is a statistical inversion method: it samples a suitable space of spectral functions looking for models compatible with the QMC data $F(q,\tau)$ via a stochastic search scheme relying on genetic algorithms.

3. Simulation details and results

In our simulations of ^{4}He in 2D we have used as interatomic potential $v(r)$ the 1979 Aziz potential [1] and N = = 120 number of atoms with periodic boundary conditions. As propagator $\mathcal{G}(\mathcal{R},\mathcal{R}',\delta\tau)$ we have used the pair–product approximation [32] with $\delta\tau = 1/160$ K^{-1}, a value that we have verified to be small enough for the adopted propagator. As projection time λ we have used $\lambda = 1.1$ K^{-1} and typical length of the simulation is $3\cdot10^6$ Monte Carlo steps (MCS); $F(q,\tau)$ has been computed over the range (1–90) $\delta\tau$. A typical run starts from a triangular lattice configuration which quickly "melts", when the density is not too large, in few thousand MCS leading to disordered configurations allowing to simulate the liquid phase without memory of the starting point. When the density is large enough the system remains in an ordered state as shown by the presence in the static structure factor $S(q)$ of sharp Bragg peaks corresponding to triangular solid ^{4}He. Only in the density range of the liquid–solid transition one gets convergence to two different states depending on the initial configuration: starting from a disordered configuration the system remains disordered whereas it remains ordered when started from the ordered configuration. The energies

of the two states take different values, the lowest one represents the stable phase and the higher energy one represents a metastable state for a single phase state.

The average value of the hamiltonian operator as a function of the density provides the equation of state of the system. We have computed the energy in a quite large range of densities both in the liquid and in the solid phase and the results are shown in Fig. 1 and listed in Tables 3 and 4 of the Appendix. The SPIGS results agree within the statistical uncertainty with the result of a Green function Monte Carlo (GFMC) computation [21]. One can also see that the SWF variational results follow quite closely the exact SPIGS results both in the liquid and in the solid phase, thus confirming the accuracy of the SWF as in the 3D case. In order to determine the melting and freezing densities, the energies have been fitted with a third degree polynomial in density in the solid phase, and a fourth degree polynomial in the liquid phase. We write the fitting function as

$$E_l(\rho) = E_0 + A\left(\frac{\rho-\rho_0}{\rho_0}\right)^2 + B\left(\frac{\rho-\rho_0}{\rho_0}\right)^3 + C\left(\frac{\rho-\rho_0}{\rho_0}\right)^4 \quad (12)$$

in the liquid phase, where a minimum energy E_0 at the equilibrium density ρ_0 is present. The last term, which is not typical in literature, turned out to be necessary in order to obtain a good fit in the whole density range here considered. On the other hand, in the solid phase we use the expression:

$$E_s(\rho) = \alpha + \beta\rho + \gamma\rho^2 + \delta\rho^3. \quad (13)$$

The obtained fitting parameters, together with their statistical uncertainties, are listed in Table 1 of the Appendix. The interpolation curves, depicted in Fig. 1, are truncated in the coexistence region, delimited by the melting and freezing densities ρ_m and ρ_f. ρ_m and ρ_f have been estimated using the Maxwell construction, and they are given in Table 2 of the Appendix.

In Fig. 2 we show some quantities like the pressure p, the chemical potential μ, the compressibility κ, and the sound velocity v_s in the liquid and in the solid phase; such quantities have been obtained from $E_0(\rho)$ via the expressions:

$$p(\rho) = \rho^2 \frac{\partial E_0(\rho)}{\partial \rho}, \quad \mu(\rho) = E_0(\rho) + p(\rho)/\rho,$$

$$\kappa(\rho) = \left(\rho \frac{\partial p(\rho)}{\partial \rho}\right)^{-1} \text{ and } v_s(\rho) = \sqrt{\frac{1}{m}\frac{\partial}{\partial \rho}\left(\rho^2 \frac{\partial E_0(\rho)}{\partial \rho}\right)}.$$

In the solid phase v_s represents the velocity of the longitudinal sound mode.

In Fig. 3 we show the SPIGS result for the static structure factor $S(q) = \langle \psi_0 | \hat{\rho}_{\mathbf{q}} \hat{\rho}_{-\mathbf{q}} | \psi_0 \rangle$ for a density close to the equilibrium one and at a density close to freezing. It is evident the emergence of more structure as the density increases towards the freezing density. Moreover, we emphasize the linear behavior of $S(q)$ for $q \to 0$ which manifests itself at very small wave vectors. This is due to the zero–point motion of long wavelength phonons [33].

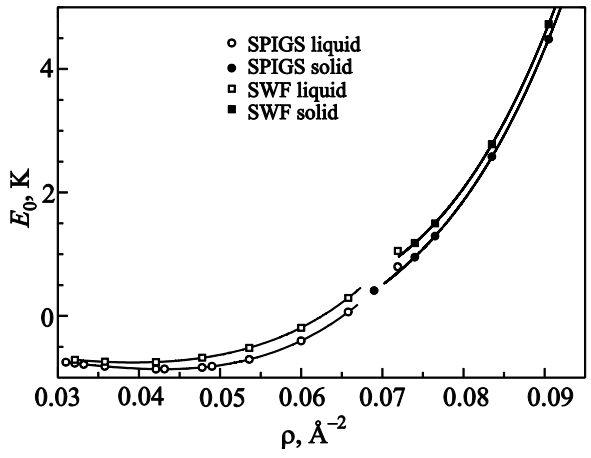

Fig. 1. Variational energies in the liquid (□) and in the solid (■) phase. Exact energies in the liquid (○) and in the solid (●) phase. The curves are the interpolated equations of state, and are truncated in the coexistence region.

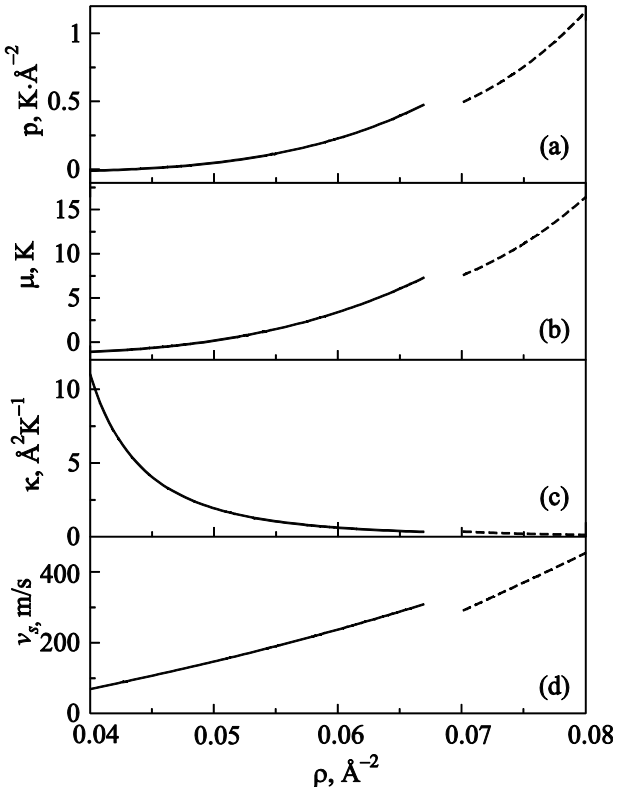

Fig. 2. Thermodynamical properties derived from the equation of state as functions of the density; liquid phase (solid line); solid phase (dashed line): pressure p (a); chemical potential μ (b); compressibility κ (c); sound velocity v_s (d).

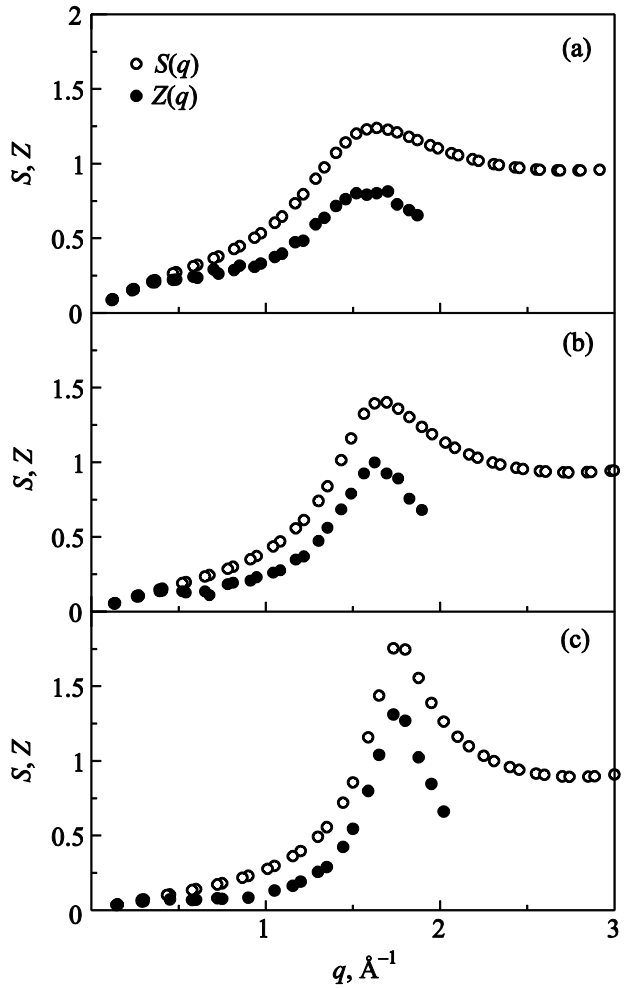

Fig. 3. SPIGS estimations of the static structure factor $S(q)$ (○) and strenght of the single particle peak $Z(q)$ (●) at the different densities ρ, Å^{-2}: 0.04315 (a), 0.0536 (b), and 0.0658 (c).

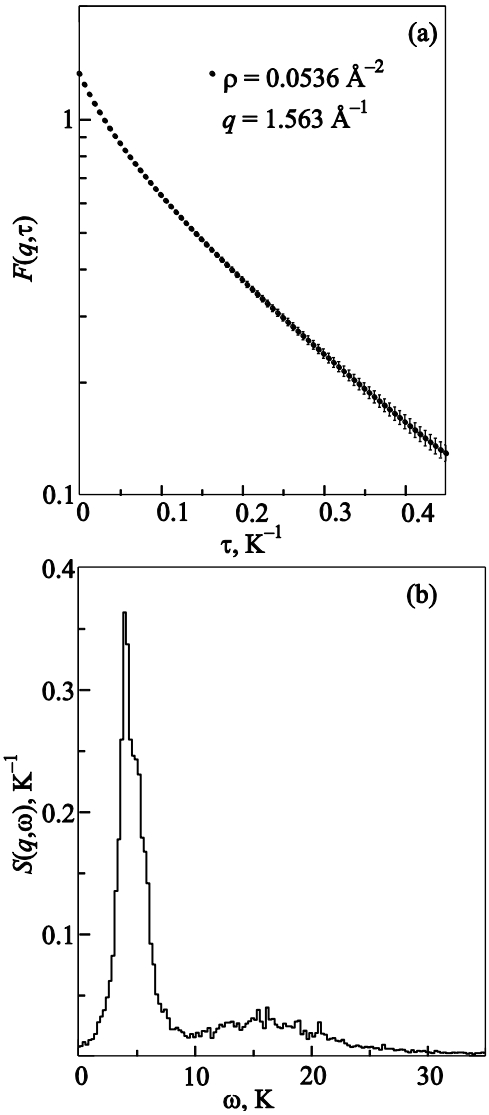

Fig. 4. An example of QMC evaluation of an imaginary time correlation function $F(q,\tau)$, defined in (10). We have plotted the τ-dependence of $F(q,\tau)$ for a given wave vector q (see the legend) in logarithmic scale to show the asymptotic single exponential behavior governed by the elementary excitation energy (a). Reconstructed $S(q,\omega)$: one can see the sharp elementary excitation peak together with the higher energy broad multiphonon contribution (b).

We have computed the dynamical correlation functions for imaginary time $F(q,\tau)$ at six densities, and namely 0.0321, 0.0421, 0.04315, 0.049, 0.0536, and 0.0658 Å^{-2} in the liquid phase. From $F(q,\tau)$, the GIFT method allows to reconstruct the dynamical structure factor of the sample, $S(q,\omega)$. An example of $F(q,\tau)$ and of the reconstructed $S(q,\omega)$ is shown in Fig. 4. $S(q,\omega)$ in general has a sharp peak in ω and this defines the energy $E(q)$ of the excitation for the given wave vector q. In addition there is a much broader peak at larger energy and this represents the so-called multiphonon contribution to $S(q,\omega)$. The elementary excitation peak in the reconstructed $S(q,\omega)$ has a finite width. This width can have two different origins. As discussed in Ref. 15, even if the system has an infinitely long-lived excitation the peak in the reconstructed $S(q,\omega)$ has a finite width because the inversion method can only identify the excitation energy with a certain uncertainty due to the limited and noisy information on $F(q,\tau)$. In this case the full width at half maximum (FWHM) can be taken as a measure of statistical uncertainty of the excitation energy. Under certain circumstances even at T = 0 K an elementary excitation acquires a finite lifetime when it can decay into two or more excitations. This happens, for instance, for the maxon excitation in superfluid ^{4}He in 3D at large pressure when the maxon energy is larger than twice the roton energy. In this case the excitation peak has an intrinsic finite linewidth and its FWHM is a measure of the inverse life-time of the excitation. Under such circumstances we expect that the width of the reconstructed $S(q,\omega)$ has also a contribution of intrinsic origin due to such physical processes, even if it is difficult to quantify precisely how large this intrinsic contribution is from the overall FWHM.

The integral over all ω of $S(q,\omega)$ is equal to the static structure factor $S(q)$. An important information is contained in the strength $Z(q)$ of the elementary excitation peak, i.e., the integral of $S(q,\omega)$ limited to the main peak. The ratio $Z(q)/S(q)$ gives the probability that in the scattering process there is emission of a single elementary excitation whereas $1-Z(q)/S(q)$ gives the probability of emission of other excitations, the so-called multiphonon processes. The behavior of $Z(q)$ is shown in Fig. 3 at three densities.

In Fig. 5 we show the obtained dispersion relation $E(q)$ for four values of the density. The reported bar represents the FWHM of the main peak in $S(q,\omega)$.

At the lowest density, 0.0321 Å^{-2}, which is near the spinodal decomposition, the excitation spectrum shows a large flat region, and a very weak roton minimum. At small wave vector the spectrum shows an anomalous dispersion, i.e., a positive curvature. At the density $\rho_0 = 0.04315$ Å^{-2} close to equilibrium the phonon–maxon–roton structure starts to be visible but maxon energy does not differ by more than 10% with respect to the roton energy. As the density further increases the maxon–roton region becomes more and more prominent until, at the highest density 0.0658 Å^{-2}, near the freezing point, the maxon energy is about three times the roton energy. At the larger density the peaks in the maxon region are quite broadened, as it is evident from the error bars in Fig. 5; we believe that in this case the linewidth largely represents an intrinsic effect due to the fact that a maxon can decay into two rotons because its energy is more than twice the roton energy. This fact is known experimentally [34] and theoretically [9,10] in 3D superfluid ^{4}He at density in the region of freezing. In Fig. 6 we plot the energy and the wave vector of roton and of maxon as function of density. It can be noticed that the roton energy in 2D (from 5.5 to 3.8 K depending on density) is significantly below the value in 3D (from 8.6 K at equilibrium to 7.2 K at freezing density). It can also be noticed that the roton wave vector has a significant density dependence while the maxon wave vector is almost density independent.

In Fig. 5 we show also the Feynman spectrum, $E_F(q) = \hbar^2 q^2/2mS(q)$, obtained using our estimation of $S(q)$. Feynman dispersion relation is accurate, as it is well known, only in the low-wave vectors region. The discrepancy between $E(q)$ and $E_F(q)$ increases with the density: $E_F(q)$ is more than twice $E(q)$ near the freezing point. We notice also that the present $E(q)$ is in good agreement with the variational result at the equilibrium density obtained using SWF in Ref. 8. At larger density the variational roton energy is about 1 K above the present result. In Fig. 7 we show more details about the low q behavior of the dispersion relation at four considered densities. It is apparent that the phononic dispersion is superlinear for the two lowest densities, and becomes sublinear at larger densities up to the freezing point. This is qualitatively similar to what happens in superfluid ^{4}He in 3D.

With respect to the strength of the quasiparticle peak $Z(q)$, at all densities $Z(q) \simeq S(q)$ at small q, i.e., the collective excitation peak almost exhausts the *f*-sum rule and multiphonon contributions are negligible. At equilibrium density the roton peak has about 2/3 of the full integrated intensity and 1/3 is due to multiphonon contribution. This multiphonon contribution is larger than in 3D and we attribute this to the fact that equilibrium density in 2D is

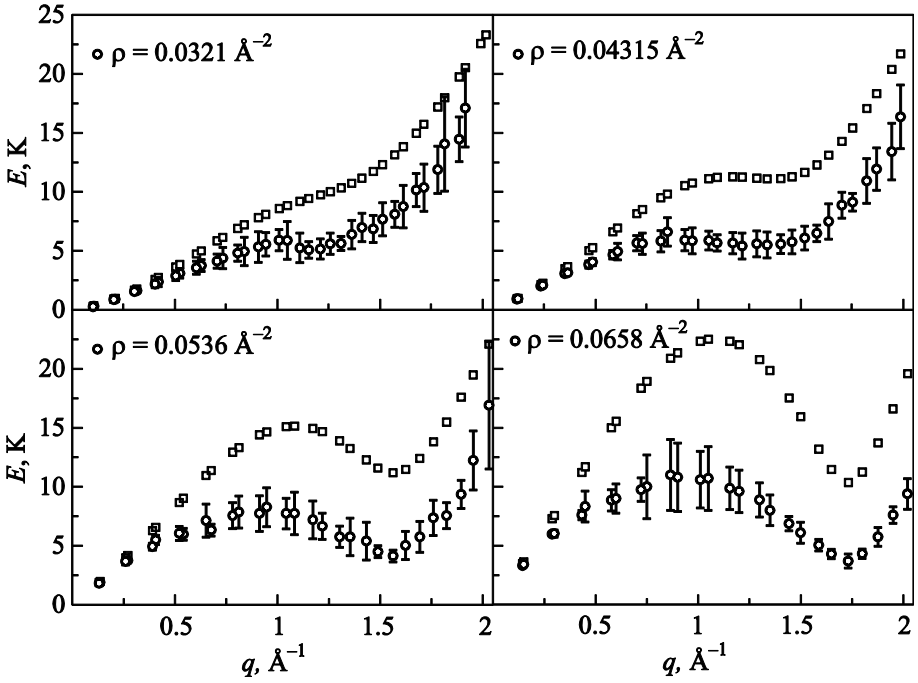

Fig. 5. Excitation spectrum from GIFT reconstructions of SPIGS evaluations of imaginary time correlation functions in the liquid phase (○), together with Feynman spectrum (□), at four densities as shown in the legends.

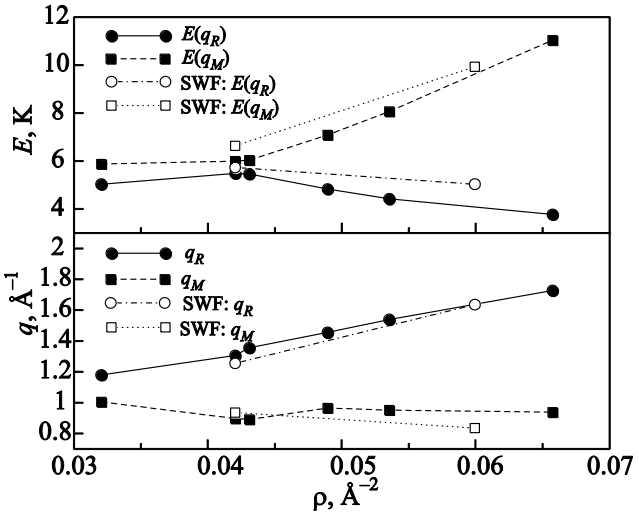

Fig. 6. Density dependence of the wave vector and of the energy of the maxon (q_M, $E(q_M)$) and the roton (q_R, $E(q_R)$) modes. Lines are guides to the eye.

rather low where short range order is not very pronounced. Only near freezing the multiphonon contribution of the roton is small (of order of 20%) as in 3D superfluid ^{4}He.

Studies of the elementary excitations of ^{4}He in restricted geometry have been performed by inelastic neutron scattering on ^{4}He confined in a number of nanopore materials. Of special relevance is a recent study [35] of ^{4}He in smooth cylindrical silica pores of diameter of about 28 Å. When the pores are filled with ^{4}He experiment shows the presence of phonon–maxon–roton excitations with a dispersion relation very similar to that of bulk ^{4}He. Such excitations are interpreted as propagating in the central part of the pore. An additional roton excitation at smaller energy is present and this is interpreted as roton confined in a compressed layer close to the cylinder wall. When the pores are only partially filled with ^{4}He the compressed layer rotons are still present, whereas the bulk-like phonon–maxon–roton branch disappears. In its place there is a modified phonon–maxon–roton brach with a decreased energy of the maxon (11 K instead of 14 K in the bulk) and a roton energy only 2 K below the maxon (the energy difference beyween maxon and roton in bulk ^{4}He is about 5 K at equilibrium density). In addition this new roton is found at a shifted wave vector, at 1.78 Å^{-1} in place of 1.92 Å^{-1} of the bulk one. This modified maxon–roton branch has been interpreted as propagating in a thin film inside the unfilled pore and connection has been made with the excitations in 2D ^{4}He as computed in Ref. 26. Indeed some similarity between the dilute layer modes of experiment and the present results for ^{4}He in 2D is present, such as the reduced energy difference between maxon and roton and a reduced wave vector q_R. On the other hand, some significant difference is present. For instance, we find $q_R \simeq 1.75$ Å^{-1} at a density close to freezing but here the roton energy is about 4 K, less than half the value of the dilute layer mode. Of course there is a difference between the present mathematical 2D system and the finite curvature of the ^{4}He film in an unfilled pore of the experiment. It is unclear if this might be the origin of that difference for the roton energy.

Finally, we obtained from the –1-moment of $S(q,\omega)$ also the static density response function, $\chi(q)$, which is shown in Fig. 8. As in 3D $\chi(q)$ is dominated by a peak at the roton wave vector. One can notice that at the equilibrium density $\chi(q)$ has an enhancement at small q which is absent in 3D [15]. This is another manifestation that the ground state of ^{4}He in 2D is at low density where atoms are not strongly coupled as in 3D.

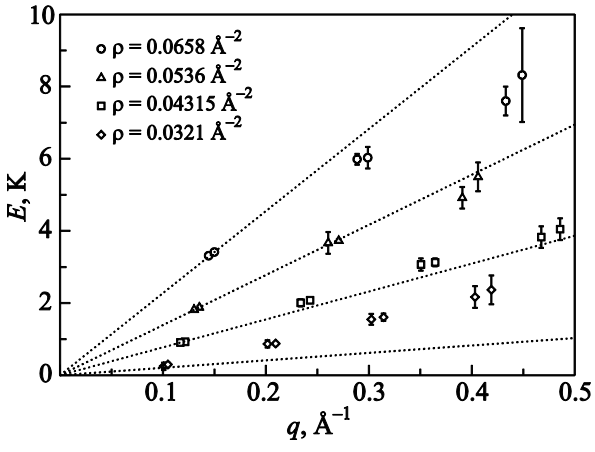

Fig. 7. Small wave vectors behavior of the estimated dispersion relation $E(q)$ for the different densities ρ, Å^{-2}: 0.0321 (◇), 0.04315 (□), 0.0536 (△) and 0.0658 (○). The dotted straight lines represent the linear behavior from which the $E(q)$ significantly deviate.

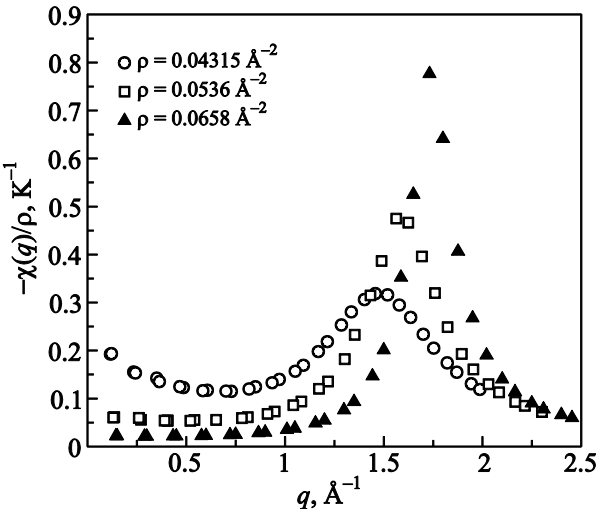

Fig. 8. Density response function extracted from the dynamical structure factor at the different densities ρ, Å^{-2}: 0.04315 (○), 0.0536 (□) and 0.0658 (▲).

4. Conclusions

We have presented the first *ab initio* QMC computation of the excitation spectrum of superfluid ^{4}He in 2D starting from exact density correlation functions in imaginary time and using advanced inversion methods to infer the dynamical structure factor $S(q,\omega)$. We find well defined excitations in the full density range of the superfluid but significant differences are present with respect to ^{4}He in 3D. In 3D the excitation spectrum over the full density range from the equilibirum density to the freezing one has a well defined phonon–maxon–roton structure with the maxon energy E_M larger by at least 50% than the roton energy Δ_R. In 2D the excitation spectrum evolves with density from maxon and roton almost coaleshing in a plateau at density close to the spinodal to a well defined maxon–roton structure at density above the equilibrium one with E_M/Δ_R becoming as large as 3 at freezing. At the same time the wave vector q_R of the roton has a strong density dependence whereas that of the maxon is almost density independent. This strong evolution with density of the shape of the excitation spectrum is due to the large density range of existence of the fluid in 2D, the freezing density is more than twice the spinodal density while in 3D the freezing density is only 60% larger than the spinodal one. At the 2D equilibrium density the maxon–roton structure is rather weak with the maxon energy only 10% larger than the roton energy. This is due to the low value of the equilibrium density so that the amount of short range order is rather small. At the same time in the phonon region there is a strong anomalous dispersion (i.e., $E(q)$ has a positive curvature). As a consequence of the shape of $E(q)$, over an extended region of q and of density, the elementary excitations are expected to have a finite lifetime even at $T = 0$ K, because they can decay into other excitations. We find evidence for this finite lifetime from our computation but the present method does not allow to quantify this.

It has been suggested [35] that the excitation spectrum of 2D ^{4}He might be relevant for the interpretation of the excitations of ^{4}He partially filling smooth cylindrical silica pores as measured by inelastic neutron scattering. We indeed find some similarity between our results and the experimental ones. However we find a strong disagreement in the value of the roton energy which is well beyond the uncertainty of the present theory. This discrepancy might be due to a curvature effect that is present in the pore but not in the present computation. It will be interesting to extend the present computation to the case of a pore geometry; present developments of QMC techniques are such that this is a feasible project.

This work has been supported by Regione Lombardia and CINECA Consortium through a LISA Initiative (Laboratory for Interdisciplinary Advanced Simulation) 2012 grant [http://www.hpc.cineca.it/services/lisa], and by a grant “Dote ricerca”: FSE, Regione Lombardia.

Appendix

In Tables 1 and 2 we give the fitting parameters of the energy as function of density with expressions (12) and (13). In our implementation of the QMC projection tecnhique, as ψ_T we use a SWF. Such a wave function, introduced by Vitiello *et al.* [36], is known to provide a very accurate description of the condensed phases of ^{4}He [37]: it has explicit pair correlations between the coordinates of the atoms as well as indirect many-body correlations via some auxiliary shadow variables, denoted $\mathcal{S} = (\mathbf{s}_1, \ldots, \mathbf{s}_N)$, which are integrated over:

$$\psi_T(\mathcal{R}) = \int \exp\left[-\sum_{i<j}^{N} u_r(r_{ij}) - \sum_{i<j}^{N} v_s(s_{ij}) - \sum_{i}^{N} c|\,\mathbf{r}_i - \mathbf{s}_i\,|^2 \right] d\mathcal{S}. \tag{A.1}$$

The pseudo-potentials are chosen to be a generalized McMillian form $u_r(r_{ij}) = (b/r_{ij})^m$, whereas the one for the shadow variables is chosen of the Aziz rescaled form $v_s(s_{ij}) = \alpha v(\delta s_{ij})$. This SWF has the same form used by Grisenti and Reatto [26] but as power m we have used $m = 6$ because this values improves the energy compared to $m = 5$ used in [37]. We have optimized the trial wave function (A.1) varying the remaining variational parameters b, α, δ and c through variational Monte Carlo simulations for various densities. Notice that the form of ψ_T is the same for the liquid and for the solid, only the variational parameters take different values. The optimized SWF is used as trial wave function for exact simulations at the same densities: the exact technique is named SPIGS method [28,29].

Table 1. Values of the fit parameters for fitting functions (12) and (13) of the variational equation of state

E_0, K	–0.753(3)	α, K	–15.2±28%
ρ_0, Å^{-2}	0.0393(2)	β, K·Å^2	765±20%
A, K	1.39(6)	γ, K·Å^4	–13311±13%
B, K	0.7(3)	δ, K·Å^6	80497±8.5%
C, K	0.93(15)		
ρ_f, Å^{-2}	0.0677	ρ_m, Å^{-2}	0.0721

Table 2. Values of the fit parameters for fitting functions (12) and (13) of the exact equation of state

E_0, K	–0.862(1)	α, a.u.	–25.1±
ρ_0, Å^{-2}	0.0430(1)	β, K·Å^2	765±20%
A, K	2.00(3)	γ, K·Å^4	–13311±13%
B, K	2.1(1)	δ, K·Å^6	80497±8.5%
C, K	0.52(14)		
ρ_f, Å^{-2}	0.0674	ρ_m, Å^{-2}	0.0701

Table 3. Optimal values of the variational parameters for the SWFs at various densities in the liquid phase, along with the values of the energy, computed both with variational and exact methods. The results are compared with previous Green function Monte Carlo results E_{GFMC} of reference [21]

ρ, Å^{-2}	*b*, Å	*c*, Å^{-2}	δ, K	α	E_{var}, K	E_{SPIGS}, K	E_{GFMC}, K
0.0310						–0.750(3)	
0.0321	2.700	0.710	0.042	0.918	–0.710(1)	–0.765(2)	–0.78(2)
0.0332						–0.787(3)	
0.0358	2.715	0.720	0.042	0.920	–0.739(2)	–0.816(2)	–0.81(1)
0.0421	2.720	0.710	0.044	0.920	–0.747(2)	–0.862(2)	–0.85(3)
0.04315						–0.861(2)	
0.0478	2.720	0.700	0.044	0.920	–0.675(2)	–0.835(3)	
0.0490						–0.817(2)	
0.0536	2.720	0.700	0.043	0.900	–0.516(3)	–0.704(2)	–0.67(3)
0.0600	2.715	0.660	0.042	0.870	–0.189(3)	–0.404(2)	
0.0658	2.710	0.645	0.042	0.840	–0.295(2)	–0.065(3)	–0.01(4)
0.0719	2.710	0.535	0.042	0.820	1.057(3)	–0.798(3)	0.82(4)

Table 4. Optimal values of the variational parameters for the SWFs at various densities in the solid phase, along with the values of the energy, computed both with variational and exact methods. The results are compared with previous Green function Monte Carlo results E_{GFMC} of reference [21].

ρ, Å^{-2}	*b*, Å	*c*, Å^{-2}	δ, K	α	E_{var}, K	E_{SPIGS}, K	E_{GFMC}, K
0.0690						0.441(5)	
0.0740	2.705	0.470	0.183	0.810	1.186(2)	0.951(2)	
0.0765	2.710	0.500	0.184	0.835	1.504(3)	1.292(3)	1.30(2)
0.0835	2.700	0.650	0.182	0.860	2.789(3)	2.579(2)	2.78(7)*
0.0905	2.710	0.700	0.183	0.880	4.733(2)	4.483(2)	4.91(3)*
0.0975	2.705	0.800	0.182	0.900	7.520(3)	7.223(3)	

Comment: values with "*" are computed near the given density.

For reference purpose we give the optimal values of the SWF variational parameters in Tables 3 and 4 for the liquid and solid phases, respectively. The values of the exact and of the variational energy are also given in that tables.

1. R.A. Aziz, V.P.S. Nain, J.S. Carley, W.L. Taylor, and G.T. McConville, *J. Chem. Phys*. **70**, 4330 (1979).
2. A.J. Leggett, *Rev. Mod. Phys*. **71**, S318 (1999).
3. L.D. Landau, *J. Phys. USSR* **5**, 71 (1941); *J. Phys. USSR* **11**, 91 (1947).
4. R.P. Feynman, *Phys. Rev*. **90**, 1116 (1953).
5. D.G. Henshaw and A.D.B. Woods, *Phys. Rev*. **121**, 1266 (1961).
6. M. Cohen and R.P. Feynman, *Phys. Rev*. **120**, 1189 (1956).
7. E. Manousakis and V.R. Pandharipande, *Phys. Rev. B* **30**, 5062 (1984).
8. W. Wu, S.A. Vitiello, L. Reatto, and M.H. Kalos, *Phys. Rev. Lett*. **67**, 1446 (1991).
9. D.E. Galli, E. Cecchetti, and L. Reatto, *Phys. Rev. Lett*. **77**, 5401 (1996).
10. L. Reatto and D.E. Galli, *Int. J. Mod. Phys. B* **13**, 607 (1999).
11. R.P. Feynman, *Statistical Mechanics*, W.A. Benjamin Inc., New York (1972).
12. R.N. Silver, D.S. Sivia, and J.E. Gubernatis, *Phys. Rev. B* **41**, 2380 (1990).
13. M. Boninsegni and D.M. Ceperley, *J. Low Temp. Phys*. **104**, 339 (1996).
14. S. Baroni and S. Moroni, *Phys. Rev. Lett*. **82**, 4745 (1999).
15. E. Vitali, M. Rossi, L. Reatto, and D.E. Galli, *Phys. Rev. B* **82**, 174510 (2010).
16. A.W. Sandvik, *Phys. Rev. B* **57**, 10287 (1998); O.F. Syljuåsen, *Phys. Rev. B* **78**, 174429 (2008).
17. M. Rossi, E. Vitali, L. Reatto, and D.E. Galli, *Phys. Rev. B* **85**, 014525 (2012).
18. M. Nava, D.E. Galli, M.W. Cole, and L. Reatto, *J. Low Temp. Phys*., *DOI 10.1007/s10909-012-0770-9* (2012).
19. J.M. Kosterlitz and D.J. Thouless, *J. Phys. C* **5**, 124 (1972).
20. D.J. Bishop, and J.D. Reppy, *Phys. Rev. Lett*. **40**, 1727 (1978).
21. P.A. Whitlock, G.V. Chester, and M.H. Kalos, *Phys. Rev. B* **38**, 2418 (1988).
22. B.E. Clernents, E. Krotscheck, and C.J. Tymczak. *Phys. Rev. B* **53** 12253 (1996).

23. H.J. Lauter, H. Godfrin, and P. Leiderer, *J. Low Temp. Phys*. **87**, 425 (1992).
24. M.W. Cole, D.R. Frankl, and D.L. Goodstein, *Rev. Mod. Phys*. **53**, 199 (1981).
25. B.E. Clements, H. Forbert, E. Krotscheck, H.J. Lauter, M. Saarela, and C.J. Tymczak, *Phys. Rev. B* **50**, 6958 (1994).
26. R.E. Grisenti, and L. Reatto, *J. Low Temp. Phys*. **109**, 477 (1997).
27. A. Sarsa, K.E. Schmidt, and W.R. Magro, *J. Chem. Phys*. **113**, 1366 (2000).
28. D.E. Galli and L. Reatto, *Mol. Phys*. **101**, 1697 (2003).
29. D.E. Galli, and L. Reatto, *J. Low Temp. Phys*. **136**, 343 (2004).
30. M. Nava, A. Motta, D.E. Galli, E. Vitali, and S. Moroni, *Phys. Rev. B* **85**, 184401 (2012).
31. M. Rossi, M. Nava, L. Reatto, and D.E. Galli, *J. Chem. Phys*. **131**, 154108 (2009).
32. D.M. Ceperley, *Rev. Mod. Phys*. **67**, 279 (1995).
33. L. Reatto and G.V. Chester, *Phys. Rev*. **155**, 88 (1967).
34. R.A. Cowley and A.D.B. Woods, *Can. J. Phys*. **49**, 177 (1971); A.D.B. Woods and R.A. Cowley, *Rep. Prog. Phys*. **36**, 1135 (1973).
35. T.R. Prisk, N.C. Das, S.O. Diallo, G. Ehlers, A.A. Podlesnyak, N. Wada, S. Inagaki, and P.E. Sokol, *arXiv:1211.0350*.
36. S.A. Vitiello, K.J. Runge, and M.H. Kalos, *Phys. Rev. Lett*. **60**, 1970 (1988).
37. B. Krishnamachari and G.V. Chester, *Phys. Rev. B* **61**, 9677 (2000).